IEEE Access
Multidisciplinary ⋮ Rapid Review ⋮ Open Access Journal

Received August 20, 2021, accepted September 14, 2021, date of publication September 28, 2021, date of current version October 6, 2021.

Digital Object Identifier 10.1109/ACCESS.2021.3115998

Impact of Amplification and Regeneration Schemes on the Blocking Performance and Energy Consumption of Wide-Area Elastic Optical Networks

ASTRID LOZADA[1], FELIPE CALDERÓN[2], JOSÉ NÚÑEZ KASANEVA[3], DANILO BÓRQUEZ-PAREDES[4], RICARDO OLIVARES[1], ALEJANDRA BEGHELLI[5], NICOLÁS JARA[1], (Member, IEEE), ARIEL LEIVA[2], (Member, IEEE), AND GABRIEL SAAVEDRA[3], (Member, IEEE)

[1]Department of Electronic Engineering, Universidad Técnica Federico Santa María, Valparaíso 2390123, Chile
[2]School of Electrical Engineering, Pontificia Universidad Católica de Valparaíso, Valparaíso 2362804, Chile
[3]Department of Electrical Engineering, Universidad de Concepción, Concepción 4070409, Chile
[4]Faculty of Engineering and Sciences, Universidad Adolfo Ibáñez, Santiago 7941169, Chile
[5]Department of Electronic and Electrical Engineering, University College London, London WC1E 7JE, U.K.

Corresponding author: Astrid Lozada (astrid.lozadav@sansano.usm.cl)

This work was supported in part by DI-PUCV 039.382/2021, in part by USM PI_LII_2020_74, in part by USM PIIC 007/2021, in part by the Agencia Nacional de Investigación y Desarrollo (ANID) Fondo Nacional de Desarrollo Científico y Tecnológico (FONDECYT) Iniciación 11190710, in part by ANID FONDECYT Iniciación 11201024, in part by ANID Doctorado Nacional/2021-21211075, and in part by ANID Magister Nacional/2021-22210736.

ABSTRACT This paper studies the physical layer's impact on the blocking probability and energy consumption of wide-area dynamic elastic optical networks (EONs). For this purpose, we consider five network configurations, each named with a network configuration identifier (NCI) from 1 to 5, for which the Routing, Modulation Level, and Spectrum Assignment (RMLSA) problem is solved. NCI 1-4 are transparent configurations based on all-EDFA, hybrid Raman/EDFA amplifiers (with different Raman gain ratio Γ_R), all-DFRA, and alternating span configuration (EDFA and DFRA). NCI 5 is a translucent configuration based on all-EDFA and 3R regenerators. We model the physical layer for every network configuration to determine the maximum achievable reach of optical signals. Employing simulation, we calculate the blocking probability and the energy consumption of the different network configurations. In terms of blocking, our results show that NCI 2 and 3 offer the lowest blocking probability, with at least 1 and 3 orders of magnitude of difference with respect to NCI 1 and 5 at high and low traffic loads, respectively. In terms of energy consumption, the best performing alternatives are the ones with the worst blocking (NCI 1), while NCI 3 exhibits the highest energy consumption with NCI 2 $\Gamma_R = 0.75$ following closely. This situation highlights a clear trade-off between blocking performance and energy cost that must be considered when designing a dynamic EON. Thus, we identify NCI 2 using $\Gamma_R = 0.25$ as a promising alternative to reduce the blocking probability significantly in wide-area dynamic EONs without a prohibitive increase in energy consumption.

INDEX TERMS Elastic optical networks, resource assignment, translucent configuration, transparent configuration.

I. INTRODUCTION

Elastic Optical Network (EON) architectures were proposed as a new paradigm to overcome the potential capacity crunch of legacy wavelength division multiplexing (WDM) networks [1], [2]. EONs divide the frequency spectrum into small slot units (Frequency Slot Units - FSU), usually of 12.5 or 6.25 GHz spectral width [3], which are flexibly allocated to the different traffic demands [4]. In this way, spectral resources are managed more efficiently than current fixed

The associate editor coordinating the review of this manuscript and approving it for publication was Bijoy Chand Chand Chatterjee.

grid WDM networks. When dynamically operated (connection requests are established on-demand and released after transmission [5]), EONs also have the potential of improving resource utilization in contrast to static operation (resources permanently allocated to each connection [6]). In this work, we focus on dynamic EON architectures.

One of the main tasks dynamic EON operators must solve is resource allocation. That is, finding a path, a modulation format suitable for the path length, and a portion of the optical spectrum on the path that meets the contiguity and continuity constraints, known as the Routing, Modulation Level, and Spectrum Assignment (RMLSA) problem [4]. Usually, the performance of RMLSA solutions for dynamic networks is contrasted in terms of the blocking ratio [6]. Thus, an RMLSA solution is better than another if it consistently exhibits a lower blocking ratio for different scenarios. In wide-area dynamic EON, there are two primary sources of blocking: a lack of capacity to establish connections and the inability to provide an acceptable quality-of-transmission (QoT) to the network connection, despite capacity availability [5], [7]–[9]. The former case arises when there are effectively no available slots to meet the requested bandwidth or having available slots these cannot be used due to spectrum fragmentation, which occurs when the available slots are isolated and they are neither continuous along the optical path nor contiguous on the spectrum domain [10], [11]. The latter case arises when the length of the route is such that the accumulation of physical layer impairments (PLI), such as amplified spontaneous emission (ASE) noise from optical amplifiers and nonlinear distortions from Kerr nonlinearity, degrade the signal-to-noise ratio (SNR) and thus, the bit-error-rate (BER), beyond acceptable limits. As in [9], we term these types of blocking as *capacity blocking* and *reach blocking*, respectively.

Standard approaches to solve the RMLSA problem establish end-to-end all-optical communication (i.e., transparent) relying only on erbium-doped fiber amplifiers (EDFAs) to compensate losses between source and destination nodes [5], [7], [8], [12]–[16]. In these cases, reach blocking has been the central problem in wide-area networks [5], [7]–[9]. This situation can be mitigated by increasing the maximum transmission reach of optical signals. Most alternatives include equipping the network with distributed fiber Raman amplifiers (DFRA) or hybrid Raman/EDFA fiber amplifiers (HFA) [17], and 3R (re-amplification, re-timing, and re-shaping) signal regeneration in some (or all) network nodes [9], [18]. There have been other proposals to extend optical transmission reach [19], [20], but they do not outperform the use of HFA [20], or may not be practical to implement [19].

Previous works studying amplification schemes and regeneration in optical networks have either focused on:

- 3R regenerators/HFA placement or assignment techniques for improving network performance or minimizing network cost [18]–[23],
- impact evaluation of different amplification schemes or 3R regeneration on the network performance, assuming a given placement technique [9], [24]–[27].

In the first case, strategies that selectively upgrade EDFA-based line optical amplifiers to HFA to reduce network cost (in terms of the required number of 3R regenerators) [20], [22] or blocking probability [19] have been proposed in fixed-grid WDM network scenarios. In EON scenarios, various algorithms have been proposed to solve the regenerator placement problem aiming to reduce power consumption [18] or reducing blocking probability [21]. Additionally, a solution for the regenerator assignment problem in dynamic EONs was proposed in [23], aiming to minimize the number of 3R regenerators and frequency slots used.

In the second case, previous studies demonstrate that the use of HFA reduces spectral occupancy (i.e., more connections can be accommodated with the same capacity) compared to pure EDFA in static EON architectures [24], [25]. In dynamic EON scenarios, it has been shown that the blocking probability can be decreased using 3R regenerators [9], [26]. However, the addition of regeneration devices exhibits diminishing returns in terms of blocking gain [27].

To the best of the authors' knowledge, previous research has not compared the performance of pure amplification schemes and the use of 3R regenerators in dynamic EON architectures. Neither have they evaluated the trade-off between the performance and cost of both cases. Such research can be beneficial for network operation and design by providing elements that help the decision-making related to what devices to deploy to increase optical reach in elastic optical networks.

In this work, we study the impact of using different amplification schemes and 3R regeneration on the blocking probability, energy consumption, and spectral and energy efficiency of dynamic EONs on two network configurations: transparent and translucent. The transparent network configuration used different amplification schemes (all-EDFA, HFA, or all-DFRA) without 3R regenerators, while the translucent one uses only 3R regenerators and EDFAs. The comparative study models the physical layer for all network configurations determining optical signals' maximum transmission reach. This information is then fed to an RMLSA algorithm operating in a dynamic scenario. As a case study, we quantify the network performance of the different configurations in the NSFNet and UKNet topologies.

The remainder of this paper is structured as follows: Section II describes the physical layer model used in this work. Next, Section III presents the methodology used to compare the different network configuration scenarios, which includes the performance metrics, the RMLSA algorithm and, the network simulator tool. Numerical results are then presented in Section IV. Finally, conclusions and remarks are provided in Section V.

II. PHYSICAL LAYER MODEL

This section describes the amplification and regeneration network configurations studied throughout this work and the model used to calculate the maximum achievable reach of optical signals.

A. NETWORK CONFIGURATIONS

We consider five different network configurations, each associated with a network configuration identifier (NCI). Configurations 1-4 correspond to transparent configurations, and configuration 5 is translucent.

a: TRANSPARENT CONFIGURATIONS

In transparent configurations, information is transmitted from source to destination entirely in the optical domain, implying that all intermediate operations, such as switching and amplification, are optical. Fig. 1 **(a)** shows a schematic of the transparent link configuration: the signal is optically transmitted through N spans with switching occurring at intermediate nodes if required. Each span is a segment (typically between 80 and 100 km long) made of standard single-mode fiber (SSMF) plus one amplification point. Although this figure only shows one switching point (OXC box in the middle of the two depicted spans), a signal can be switched at several points along the path or not switched at all if an optical fiber link directly connects the source and destination nodes. Optical amplification for one span can have one of the following configurations:

- *NCI* 1 (all-EDFA): at the end of each span an EDFA is placed to compensate for the losses, as shown in Fig. 1 **(b)**.
- *NCI* 2 (HFA): a Raman pump provides distributed Raman gain G_R, followed by an EDFA with gain G_E, recovering the residual loss. The total gain of the HFA is $G = G_R G_E$. This configuration is shown in Fig. 1 **(c)**, characterized by the Raman gain ratio (Γ_R) corresponding to the percentage of the total gain (in dB) compensated by the Raman amplifier. Note that the cases when $\Gamma_R = 0$ and $\Gamma_R = 1$ correspond to all-EDFA and all-DFRA, respectively.
- *NCI* 3 (all-DFRA): a Raman pump is used to provide gain in each span, as shown in Fig. 1 **(d)**.
- *NCI* 4 (alternating spans): one span uses EDFA and the one immediately after uses DFRA, as shown in Fig. 1 **(e)**.

b: TRANSLUCENT CONFIGURATION

In translucent communications, data is transmitted from source to destination using at least one optoelectronic conversion device. In our case, we use 3R regeneration devices for increasing the optical reach in intermediate nodes, as displayed in Fig. 2. Therefore, the fifth and last configuration is as follows:

- *NCI* 5 (translucent): the information transmitted from source to destination is regenerated in an intermediate node using a 3R regenerator equipped with optoelectronic conversion. As shown in Fig. 2, in this configuration, all-EDFA is used in each span.

The configurations selected for this study were chosen for the following reasons: NCI 1 because EDFA is the most used technology for the deployment of optical links [28], NCI 2 and 3 due to the benefits presented by Raman amplification in hybrid schemes and to a greater extent individually, in terms of noise accumulation [17], [29], NCI 4 as an intermediate alternative between NCI 1 and 3 with improved blocking rate without significant energy consumption increase, and NCI 5 with all-EDFA amplification in order to avoid combining two elements with high energy consumption and costs such as regenerators and DFRA [18]–[20].

B. OPTICAL TRANSMISSION REACH MODEL

We assumed that signals are degraded by ASE and nonlinear interference (NLI) noise to calculate the maximum distance achievable by any given modulation format. Other fiber impairments, such as chromatic and polarization mode dispersion, are assumed to be compensated for using digital signal processing [30]. Furthermore, we assume that all network components are carefully designed to avoid any additional sources of signal degradation.

We evaluate the signal QoT of each optical path in terms of its received SNR [30]:

$$SNR = \frac{P_{in}}{P_{ASE} + \psi_{NLI} P_{in}^3}, \tag{1}$$

where P_{in} is the input signal power, P_{ASE} is the ASE noise power over the signal bandwidth, and ψ_{NLI} is the NLI coefficient.

The total ASE noise at the receiver was calculated using [31]:

$$P_{ASE} = N_s F_{eq} h\nu \Delta_{ref} (G - 1), \tag{2}$$

where N_s is the number of spans, F_{eq} is the equivalent amplifier noise figure, h is Planck's constant, ν is the carrier frequency, Δ_{ref} is the signal bandwidth and G is the amplifier gain.

For each amplifier configuration F_{eq} takes a different value. We denote by F_{EDFA}, F_{DFRA}, and F_{HFA} [32] the equivalent noise figure of the EDFA, DFRA, and HFA amplifiers, respectively. The right column of Table 1 shows the values used for F_{EDFA}, F_{DFRA} and F_{HFA}. F_{EDFA} is used in NCI 1 and NCI 5 for each span and in NCI 4 for spans using EDFA. F_{HFA} is used in NCI 2 for each span, depending on Γ_R value. F_{DFRA} is used in NCI 3 in each span and NCI 4 in spans using DFRA. In every network configuration (NCI 1 - 5), the amplifiers were set to compensate for the loss of one span and include a 2 dB of margin, thus $G = exp(\alpha L) \cdot 1.58$, where α is the fiber attenuation coefficient, and L is the span length. The values of α and L can be found in the left column of Table 1. Finally, for calculating the maximum distance achievable by optical signals, it is assumed that links are made of identical fiber spans.

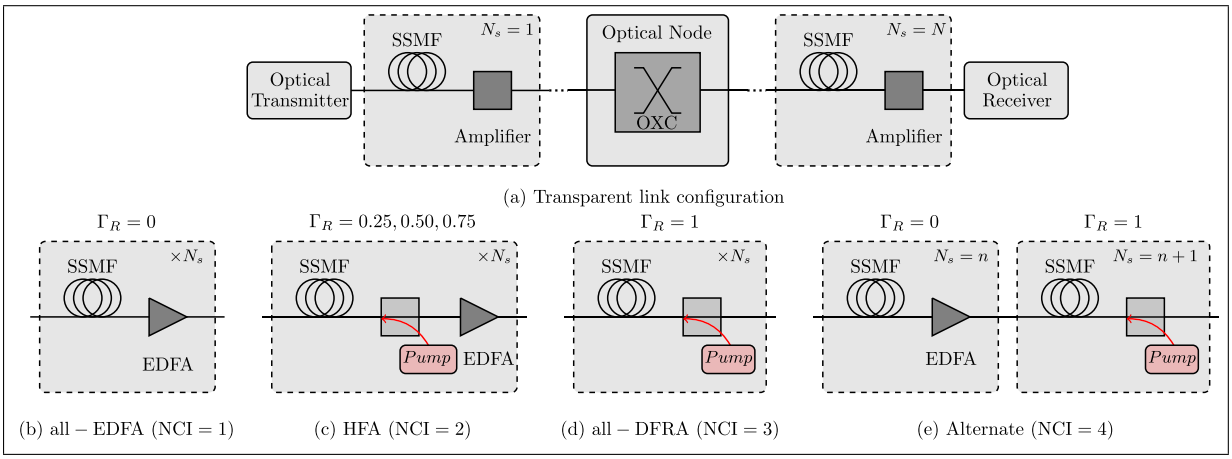

FIGURE 1. Transparent configuration. (a) Transparent link configuration. (b)-(e) Span configuration for different amplification configurations (NCI 1-4).

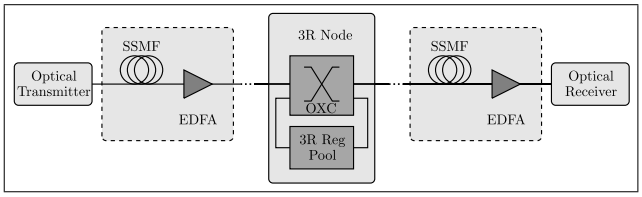

FIGURE 2. Translucent link configuration (NCI 5).

The NLI coefficient, ψ_{NLI}, is given by the product $N_s\psi_{NLI}^{1\ span}$ [30], [33] assuming incoherent NLI accumulation, where $\psi_{NLI}^{1\ span}$ is the NLI coefficient in a single span. The ψ_{NLI} coefficients were estimated using the conventional GN model [30] when EDFA amplification is used (NCI 1, 4 and 5) and a closed-form approximation from [29] for the configurations using HFA (NCI 2) and DFRA (NCI 3 and 4). The right column of Table 1 lists the value of ψ_{NLI} for 1 span for the different network configurations. We denote by $\psi_{NLI-EDFA}$, $\psi_{NLI-DFRA}$ and $\psi_{NLI-HFA}$ the NLI coefficients when EDFA, DFRA, and HFA amplification is used, respectively. The value $\psi_{NLI-EDFA}$ is used in each span in NCI 1 and NCI 5 and only in the spans using EDFAs in NCI 4. The value $\psi_{NLI-HFA}$ is used in each span in NCI 2, according to the value of Γ_R. Finally, the value $\psi_{NLI-DFRA}$ is used in each span in NCI 3, and in the spans using DFRA in NCI 4. Since the value of the NLI coefficient depends on the optical bandwidth used, the calculation of it considered a fully-loaded C-band with an optical bandwidth of 4 THz divided in 320 FSUs of 12.5 GHz each.

PM-QPSK, PM-16-QAM, and PM-64-QAM are the available modulation formats within the flexible transceivers, each with a target pre-FEC BER of $4.7 \cdot 10^{-3}$ using 6.25% overhead [34]. In this case, the bit rates allowed by each modulation format on an optical channel with a bandwidth of one FSU are 46, 92, and 140 Gb/s for PM-QPSK, PM-16-QAM and PM-64-QAM, respectively.

TABLE 1. Fiber parameters for maximum achievable reach calculation for every NCI.

Fiber and signal parameters		*Amplifier parameters*	
α	0.0507 Np/km	F_{EDFA}	5 dB
α_p	0.0553 Np/km	$F_{HFA-\Gamma_R=0.25}$	1.12 dB
β_2	-21.3 ps^{2}km^{-1}	$F_{HFA-\Gamma_R=0.50}$	-1.52 dB
γ	1.3 W^{-1}km^{-1}	$F_{HFA-\Gamma_R=0.75}$	-3.33 dB
Δ_{ref}	12.5 GHz	F_{DFRA}	-4.71 dB
L	100 km	g_R	0.4 W^{-1}km^{-1}
v	193.5 THz	$\psi_{NLI-EDFA}^{1\ span}$	0.0097 mW^{-2}
R	12.5 GBaud	$\psi_{NLI-HFA(\Gamma_R=0.25)}^{1\ span}$	0.0105 mW^{-2}
BW	320 FSUs	$\psi_{NLI-HFA(\Gamma_R=0.50)}^{1\ span}$	0.0106 mW^{-2}
		$\psi_{NLI-HFA(\Gamma_R=0.75)}^{1\ span}$	0.0113 mW^{-2}
		$\psi_{NLI-DFRA}^{1\ span}$	0.0149 mW^{-2}

The maximum achievable reach (MAR) for each modulation format was defined as the maximum distance that the optical signal can be transmitted at optimum power before exceeding the target BER. Based on that target BER, the SNR thresholds for each modulation format were determined: 8.5, 15.5, and 21 dB for PM-QPSK, PM-16-QAM, and PM-64-QAM, respectively. The calculated MAR values for the available modulation formats are listed in Table 2. The values reported have been rounded down to the closest multiple of the span length. The MAR represents the distance constraint in the modulation level selection in the RMLSA algorithm. All fiber parameters used for the calculations of the maximum achievable reach used throughout this work are listed in Table 1 where parameters α_p, β_2, γ, R, and g_R are the pump attenuation coefficient, group velocity dispersion coefficient, nonlinear coefficient, symbol rate, and Raman gain coefficient, respectively.

III. METHODOLOGY

In this section, we describe the methodology used for the comparison of NCI 1-5, described in Section II. The network performance metrics are described in Subsection III-A (blocking probability, energy consumption, and spectral and

TABLE 2. Maximum achievable reach (in km) for various modulation formats, using BER = $4.7 \cdot 10^{-3}$ and 320 FSUs optical bandwidth for every NCI.

Modulation format	*NCI* 1, 5 $\Gamma_R = 0$	*NCI* 2 $\Gamma_R = 0.25$	*NCI* 2 $\Gamma_R = 0.50$	*NCI* 2 $\Gamma_R = 0.75$	*NCI* 3 $\Gamma_R = 1$	*NCI* 4 *Alternate*
PM-QPSK	2900	5200	7800	10100	11400	4600
PM-16-QAM	500	1000	1500	2000	2200	800
PM-64-QAM	100	200	400	500	600	200

energy efficiency). The RMLSA algorithm and the simulation scenario are explained in subsections III-B and III-C, respectively.

A. PERFORMANCE METRICS

We define three performance metrics for evaluating all amplification/regeneration configurations on dynamic elastic optical networks.

1) BLOCKING PROBABILITY

The network must be designed so that the blocking probability does not exceed a threshold value. In wide-area elastic optical networks, a request can be blocked due to one of the following situations: First, lack of available resources (FSUs) on the selected path. Second, the selected route has enough FSUs to accommodate the request, but the optical signal cannot reach the destination since it does not meet the quality of transmission (QoT) required. We term these two blocking events as Capacity Blocking ($\mathcal{CB}$) and Reach Blocking ($\mathcal{RB}$), respectively.

Blocking events are recorded as follows. First, resource availability is checked. If resources are not available, the request is considered to be blocked due to the lack of capacity, and QoT is not evaluated. Once resource availability has been confirmed, QoT is evaluated. If the QoT requirements are not met, the request will be blocked and the event will be recorded as a reach blocking event. In this way, the overall blocking probability ($\mathcal{B}$) can be computed as the sum of these two blocking events:

$$\mathcal{B} = \mathcal{CB} + \mathcal{RB}. \tag{3}$$

2) ENERGY CONSUMPTION

The main drawback of the network configurations used to extend the reach of an optical connection described in Section II is their high energy consumption, leading to a trade-off between blocking probability and energy consumption. This work analyzes the energy consumed by each NCI configuration considering the optical amplifiers in the transparent configurations and 3R regenerators and optical amplifiers in the translucent case. We assume that the energy consumed by network elements different from amplifiers and regenerators (e.g., optical transceivers and switches) remains constant during network operation.

The total energy consumed by a given network configuration, E_{NCI}, is the sum of the energy consumed by the amplifiers and the regenerators over the observation time:

$$E_{NCI} = \sum_{span} P^e_{AMP} T + \sum_{connection} P^e_{RGN} \tau, \tag{4}$$

where the first term on the right side of the equation corresponds to the energy consumed by the optical amplifiers for a given NCI during the observation time T, and the second term is the energy consumed by all connections using a regeneration device.

In Eq. (4), P^e_{AMP} corresponds to the electrical power consumed by an optical amplifier, T is the cumulative work time, P^e_{RGN} is the electrical power consumed by a regenerator for a single connection, and τ is the holding time of the regenerated connection. Note that the amplifier power consumption is time-independent due to the fully loaded system assumption described in the physical layer model. The E_{NCI} value in Eq. (4) is expressed in Joules [J].

The power consumption of optical amplifiers depends on the network configuration selected. We use the model for HFA presented in [19], [35] which describes the behavior of all configurations studied herein. We calculate the power consumption of an optical amplifier for a single span using:

$$P^e_{AMP} = \frac{1}{\eta_{EDFA}} N_{ch} P_{ch} \left(1 - \frac{1}{G_E}\right) + \frac{N_R}{\eta_R} \frac{\ln(G_R)}{g_R L_{eff}}, \tag{5}$$

where η_{EDFA} and η_R are the power conversion efficiency for EDFA and Raman amplifiers, respectively; N_{ch} and P_{ch} are the number and power for the channels amplified by the EDFA; and N_R, g_R, and L_{eff} are the Raman pump multiplicity, Raman gain coefficient, and effective amplification length, respectively. The first term on the right side of Eq. (5) corresponds to the electrical power required to pump the EDFA section with a G_E gain value. The second term is equivalent for the Raman amplifier with a gain G_R. In all-EDFA (NCI 1) and all-DFRA (NCI 3) configurations, the second and first terms of the right side of Eq. (5) are equal to 0, respectively.

The power consumption of 3R regenerator devices varies depending on the data rate of the regenerated signal. Here we assume that a regenerator consists of a variable bandwidth receiver and a transmitter in a back-to-back configuration. The model used to describe the electrical power consumption of a regenerator as a function of the bit rate [36]–[38] is as follows:

$$P^e_{RGN} = K_1 \times B_{sd} + K_2, \tag{6}$$

where K_1 is a power scaling factor related to the transmission bit rate and the required DSP, B_{sd} is the bit rate of a connection request between nodes s and d, and K_2 is a constant consumed power related to the operation of the optical source and analog components. The values used for the constant values K_1 and K_2 depend on the studied transceiver, and different values are observed within the literature. The study from [36] is commonly used within the EON literature. In this case K_1 and K_2 correspond to 1.683 W/Gb/s and 91.3 W, respectively [36]–[40], representing a power consumption of 260 W for

a 100 Gb/s transmission. However, these values correspond to a study from 2010 [40]. Thus the advances in transceiver manufacturing are not considered. We additionally consider a CFP digital coherent optical (DCO) transceiver, where K_1 and K_2 are equal to 0.105 W/Gb/s and 21.5 W [41], [42], respectively. That presents a maximum power consumption of just 32 W for 100 Gb/s transmission, eight times lower than the power consumption of devices from 2010.

3) SPECTRAL AND ENERGY EFFICIENCY

We study the efficiency of each network configuration using the network spectral efficiency (SE) and the energy efficiency (EE) metrics. Both metrics, SE and EE, are associated with the cost incurred to operate the network for a target throughput. SE indicates how well the spectral resources of the network are utilized and EE how much energy is required to operate the network.

SE is defined as the ratio between the total network throughput and the allocated spectrum during an observation period [43]. The network throughput is calculated as the sum of the bit rates of all established connections during the observation time T. The allocated spectrum is the sum of the required bandwidth for all connections.

$$SE = \frac{\sum_{\forall(s,d)} B_{sd} \cdot \tau}{\sum_{\forall(s,d)} \Delta f_{sd} \cdot \tau}, \tag{7}$$

where Δf_{sd} is the optical bandwidth in Hz allocated to connection (s, d), equal to the number of FSUs required by connection (s, d) multiplied by the spectral width of an FSU.

EE is the energy required to achieve a given network throughput during an observation time T. It is expressed in J/s, and it represents the energy-per-bit, a fundamental unit to measure energy efficiency in digital communications [44], [45]. It was calculated as follows:

$$EE = \frac{E_{NCI}}{\sum_{\forall(s,d)} B_{sd} \cdot \tau}, \tag{8}$$

where E_{NCI} is the energy consumption of amplifiers and regenerators of a given network configuration (Eq. (4)).

B. RMLSA ALGORITHM

The RMLSA algorithm used was presented in [9]. The algorithm establishes connections taking into account a given BER threshold. Fig. 3 shows a high-level description of the main steps executed by the RMLSA algorithm. In it, connection requests generated in transparent network configurations (NCI 1-4) are processed executing Stage A only, and connection requests generated in the translucent network configuration (NCI 5) are processed executing Stages A and B.

Upon receiving a connection request between nodes s and d with a bit rate of $B_{s,d}$, the algorithm attempts to establish a transparent connection (Stage A). The algorithm looks for available capacity in the candidate K shortest paths $(K - SP_{s,d})$ in increasing order of length. These routes have been previously calculated using the Dijkstra algorithm [46]. With each attempted route, the algorithm determines the modulation format that requires the lowest number of FSUs while having an optical reach greater than or equal to the length of the selected path. Next, the spectrum allocation is performed by executing the First-Fit (FF) algorithm, which exhibits a good trade-off between performance and computational complexity [9]. If the connection cannot be established after attempting all paths, the request is rejected (for NCI 1-4), or Stage B is activated to attempt to establish a translucent connection using one regenerator in the path (for NCI 5).

In Stage B, it is assumed that all network nodes are equipped with the same number of 3R regenerators and that they are used only if a connection request cannot reach the destination due to limited MAR or if the capacity on the path is not continuous or contiguous. The algorithm attempts to establish a translucent connection in one of the K shortest paths, in increasing order of length. In that case, the path is divided into two segments as described in [9], using the regenerator allocation algorithm based on the First Longest Reach Regenerator (FLR) policy [47]. If the node between both segments has at least one regenerator available, then the algorithm allocates resources for the first segment. If this allocation is successful, then the resource assignment for the second segment is attempted. It is assumed that the regeneration device can convert the modulation format and change the spectral position if required. If the connection between the nodes s and d cannot be established using these two segments in the candidate path, the algorithm attempts establishing the connection using a new pair of segments. This procedure is repeated until the connection can be established, or all segment combinations in the candidate path have been unsuccessful. If the translucent connection cannot be established in the shortest path, Stage B is re-started considering the following shortest path until every path in $K - SP_{s,d}$ has been evaluated. If none of these attempts is successful, then the connection request is finally rejected.

C. SIMULATION SCENARIO

The network performance was evaluated using an event-driven simulator built in C++. The operation of a flexible optical network was simulated considering as inputs: the network NCI, the network topology, the FSU capacity per link, the RMLSA algorithm, the number of regenerators per node, the set of bit rates and modulation formats supported by nodes, the optical reach table (MAR) of different network configurations and the number of FSUs required by different modulation formats and bit rates (Table 3). Table 4 lists the values of all the input data parameters used in the simulation.

Each event in the simulator represents a connection request or release. Each connection request is defined by a source-destination pair and a bit rate. All possible source-destination pairs generate traffic according to an ON-OFF traffic model, that assumes limited traffic sources, in which a maximum of one connection is established between each node pair at any time. That is, if successfully established, the connection is active during the ON time. During the ON period, the source

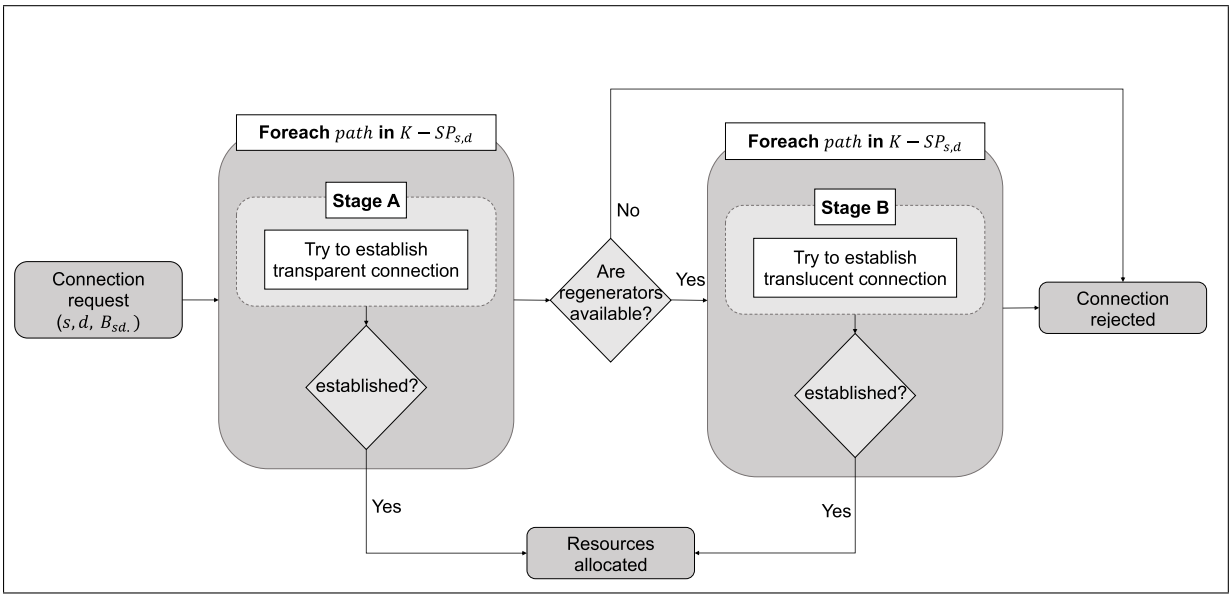

FIGURE 3. RMLSA flowchart.

transmits at the requested bit rate. After this time, a connection release event is generated, and the simulator releases the corresponding allocated resources. The connection is then inactive during the OFF time, after which a new connection request event for this specific source-destination pair is generated. Each time a new request event is generated, its bit rate is uniformly selected from the set of available bit rates listed in Table 4.

The ON and OFF periods are assumed to be exponentially distributed, with mean values denoted by τ and t_{OFF}, respectively. The network traffic load, denoted by ϱ, is given by:

$$\varrho = \frac{\tau}{\tau + t_{OFF}}. \tag{9}$$

For each value of traffic load studied, the simulator output data (number of connections established, number of connections rejected, and utilization of FSU and regenerators) is then used to calculate the blocking probability, the energy consumption, and the spectral and energy efficiency of each network configuration.

IV. RESULTS

The performance of the different network configurations NCI 1-5 was evaluated employing simulation. We use Raman gains coefficient of 0.25, 0.50 and 0.75 for NCI 2 configuration, and 1, 3, 5, and 10 3R regenerators per node for NCI 5 scenario. Network simulations were run using the NSFNet topology, shown in Fig. 4. The values of the input data required for the network simulator are summarized in Table 4. For every network configuration, the blocking probability, the energy consumption, and the spectral and energy efficiency were evaluated. Additionally, simulations

TABLE 3. Spectrum requirements in terms of FSUs for each bit rate and modulation format pair.

Modulation format	*Bit rate*				
	10 Gb/s	40 Gb/s	100 Gb/s	400 Gb/s	1000 Gb/s
PM-QPSK	1	2	4	16	40
PM-16-QAM	1	1	2	8	20
PM-64-QAM	1	1	2	6	14

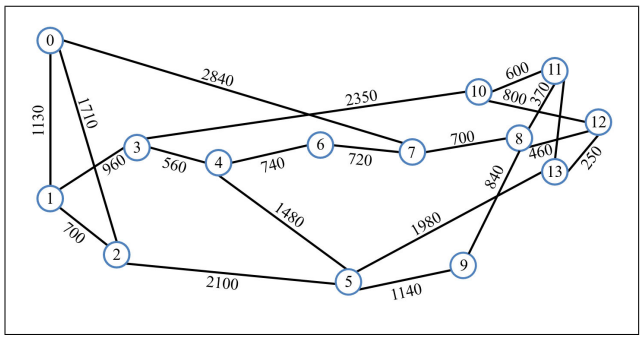

FIGURE 4. NSFNet network topology with the lengths of every optical link (in km).

were carried out using the UKNet network topology with shorter links compared to NSFNet. UKNet presents a network diameter of 1000 km. Overall, the same trend in the results for NSFNet was observed in the UKNet. Due to space constraints, in this paper, we present the results obtained for the NFSNet topology only. Data supporting the results of both network topologies can be found in https://iro-team.gitlab.io/IA3R_ext.pdf.

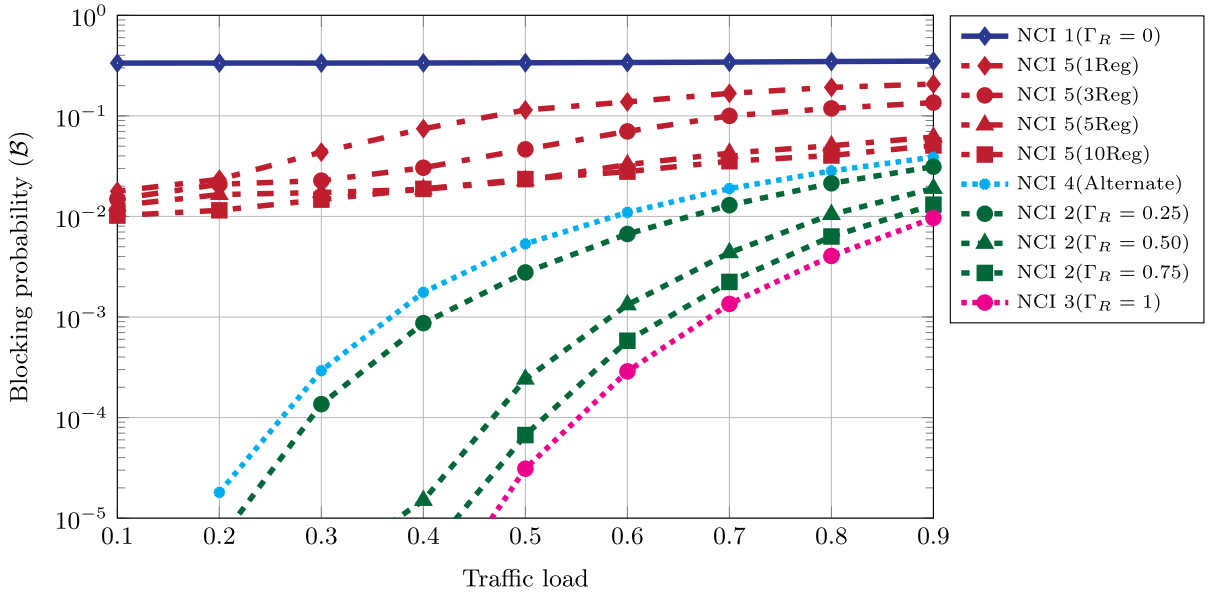

FIGURE 5. Blocking probability for the network for all network configurations.

TABLE 4. Simulation parameters.

Parameters	*Value*
Resource allocation algorithm	Fig. 3
Spectrum Requirements	Table 3
BER threshold	$4.7 \cdot 10^{-3}$
Topology	NSFNet (Fig. 4)
Number of connection requests	10^7
Traffic Load	$0.1 - 0.9$
Number of FSU by link	320
Bit rates [Gb/s]	10, 40, 100, 400 and 1000
Modulation Formats	PM-QPSK, PM-16-QAM, PM-64-QAM
MAR for all NCI	Table 2
Regeneration devices per node	1, 3, 5 and 10
T	1000 t.u
τ	1 t.u

A. BLOCKING PROBABILITY

Fig. 5 shows the network blocking probability for all the studied network configurations as a function of the traffic load.

NCI 1, based on all-EDFA amplification, exhibits the worst performance of the studied cases with an average blocking probability of $3.3 \cdot 10^{-1}$ for all traffic loads. The fact that the blocking does not change with the traffic load suggests that the main reason for blocked requests, in this case, is the limited reach offered by the modulation formats under consideration.

NCI 5 exhibits a lower blocking than NCI 1, despite having the same optical reach. The lower blocking of NCI 5 is achieved thanks to the use of 3R regenerators: some connections with limited optical reach (that would have been blocked in NCI 1) can still be established in NCI 5 by regenerating the signal at an intermediate node along the route. Besides, the better blocking performance of NCI 5 compared to NCI 1, is still worse than the remaining transparent schemes. It can be seen that although a higher number of regenerators reduces the blocking probability, the addition of more than three devices per node offers diminishing returns, and the improvement in the blocking ratio is marginal. For example, considering a traffic load of 0.3, increasing the number of regenerators per node from 3 to 10 only decreases the blocking probability from $3.0 \cdot 10^{-2}$ to $1.5 \cdot 10^{-2}$.

NCI 4, corresponding to the alternate span configuration, offers a reduced blocking probability than NCI 1 and NCI 5. For example, considering a traffic load of 0.3, the blocking probability using NCI 4 was $2.93 \cdot 10^{-4}$, almost three orders of magnitude less than NCI 1 and one order of magnitude lower than NCI 5 (average value of $2.45 \cdot 10^{-2}$). This behavior is obtained due to the increased reach for all modulation formats compared to NCI 1 and 5, as seen in Table 2.

NCI 2 and 3 present a significant improvement in the blocking probability compared to the other studied configurations. For NCI 2, 3 different Raman gain ratios (Γ_R) were studied: 0.25, 0.50 and 0.75. It can be seen that as Γ_R is increased, the blocking probability is reduced. For example, considering a traffic load of 0.3, a blocking probability of $1.36 \cdot 10^{-4}$, $3 \cdot 10^{-6}$, $4 \cdot 10^{-6}$ and $1 \cdot 10^{-6}$ was observed for a value Γ_R equal to 0.25, 0.50, 0.75 and 1, respectively. Two main reasons explain this behavior: Firstly, the increase in the MAR (see Table 2) reduces the number of connection requests blocked due to the inability to reach their destination; secondly, the extended MAR for all modulation formats allows the users to employ high order formats (that require a lower number of FSUs, as shown in Table 3) and thus, the blocking ratio is reduced due to increased spectrum availability.

Finally, we studied the source of blocking for all NCIs. Results are shown in Fig. 6. Each network configuration

3 bars are shown, corresponding (from left to right) to traffic loads of 0.3, 0.5, and 0.8, respectively. The main cause of blocking for NCI 1 is the limited MAR for all modulation formats for all studied traffic loads. Only at a traffic load of 0.8 capacity blocking is observed for NCI 1, with a value of $1.65 \cdot 10^{-2}$. On the contrary, lack of available capacity is the only cause of blocking for NCI 2, NCI 3, and NCI 4. Note that following the trend observed in Fig. 5, the blocking ratio increases with the traffic load. For NCI 2-4, the MAR is enough to establish every connection request independent of the traffic load. The blocking performance of NCI 5 is due to a mix of limited reach and capacity, but reach blocking dominates the performance. As the number of available regenerators increases, a decrease of reach blocking is observed for all traffic loads, as more connections can reach their destination using them. As reach blocking is reduced, an increment in capacity blocking is observed in NCI 5, when more connections are established in the network.

The difference in performance between the transparent (NCI 2-4) and translucent (NCI 5) solutions to improve the transmission reach is because a regenerator can only serve a single user at a time to extend its transmission reach. This situation means that only a limited number of connections can be established using regenerators, and other requests that cannot reach their destinations are blocked. On the other hand, NCI 2-4 offers lower noise accumulation across the entire available spectrum, improving the quality of service for all network users.

B. ENERGY CONSUMPTION

To evaluate the network's energy consumption, we evaluate the simulation after 1000 time units for every NCI under investigation for traffic loads of 0.3, 0.5, and 0.8. We define the duration of a single time unit as 1 second; thus, $T = 1000$ s and $\tau = 1$ s were used to evaluate the total energy consumption. As stated in Section III, only the energy consumed by the optical amplifiers and regenerators was considered for this analysis, assuming that the energy consumption of all other network elements in the different network configurations does not change. To evaluate the consumption of the amplifiers using Eq. (5) N_R was set as 2, conventionally used to pump the C-band, and power conversion efficiencies for EDFA (η_{EDFA}) and Raman (η_R) of 5% and 3% were assumed as in [35].

Fig. 7 shows the total energy consumed by amplifiers and regenerators for each network configuration, where Fig. 7 **(a)** shows the transparent cases (NCI 1-4) and Fig. 7 **(b)** shows the translucent cases (NCI 5). For NCI 1-4, the energy consumption is independent of the network's traffic load, as the amplifiers were assumed to provide gain over the entire available spectrum. NCI 1 exhibits the lowest energy consumption of 2.7 MJ due to the high power efficiency of EDFA amplifiers. NCI 2 and 3, representing scenarios with increased Raman gain ratio values, present a linear increase in consumed energy with values ranging from 5.7 to 14.1 MJ. NCI 4 exhibits an energy consumption of 9.2 MJ, comparable to NCI 2 with $\Gamma_R = 0.50$. The high energy consumption of NCI 4 arises from the spans amplified purely by the Raman amplifier. Note that this high energy consumption leads to a better blocking performance compared to NCI 1. However, it offers a higher blocking probability than any NCI 2 studied, as seen in Fig. 5.

For all network configurations using DFRA (NCI 2-4), the high energy consumption is related to the Raman gain coefficient of a single-mode fiber. As stimulated Raman scattering is a nonlinear effect, high power pumps are required to obtain signal amplification. Typically, Raman pump power can be as high as 500 mW, approximately an order of magnitude higher than EDFA pump power.

Finally, the total energy consumed by NCI 5 depends on the energy consumed by the EDFA amplifiers (same as NCI 1), the number of established connections using regenerators, and their bit rate.

In this configuration, we used two different transceiver models to evaluate the energy consumption of regenerators, as described in Section III. The blue bars in Fig. 7 **(b)** represent the energy consumption when the transceiver model from [36]–[38] is considered, called *Co-BVT* herein. This is the most common model used in previous work evaluating the energy consumption of regenerators and the values considered date from circa 2010. Additionally, the energy consumption of NCI 5 considering state-of-the-art values for the regenerator energy consumption, corresponding to CFP transceivers [41], [42] was studied, called *DCO* herein. The energy consumption of this type of regenerator is shown in red bars in Fig. 7 **(b)**. For a traffic load of 0.3, a low number of connections use the available regenerators. On increasing the number of regenerators per node from 1 to 10, no consumed energy addition is experienced, with a value of 3.6 MJ and 11 MJ for the Co-BVT and DCO transceiver models, respectively. For higher traffic loads, however, different energy consumption is observed when more regenerators are available. The consumed energy increases together with the traffic load and the number of available regenerators due to the higher number of connections using them. For a traffic load of 0.5, the consumed energy increased from 3.9 MJ to 6.1 MJ, and from 10.4 MJ to 22 MJ when 1 and 10 regenerators were available, considering the DCO and Co-BVT transceiver models, respectively.

Two main conclusions can be drawn from the energy consumption using regenerators. Firstly, the significant difference observed between the two transceiver models, which highlights the relevance of using state-of-the-art components, can greatly impact network operation costs. Secondly, the energy consumption only depends on the network traffic load in the translucent scenario, since in the transparent case, no additional equipment is needed at different traffic loads.

C. SPECTRAL AND ENERGY EFFICIENCY

Fig. 8 **(a)** shows the spectral efficiency (SE) achieved by the different network configurations for a traffic load equal to 0.3.

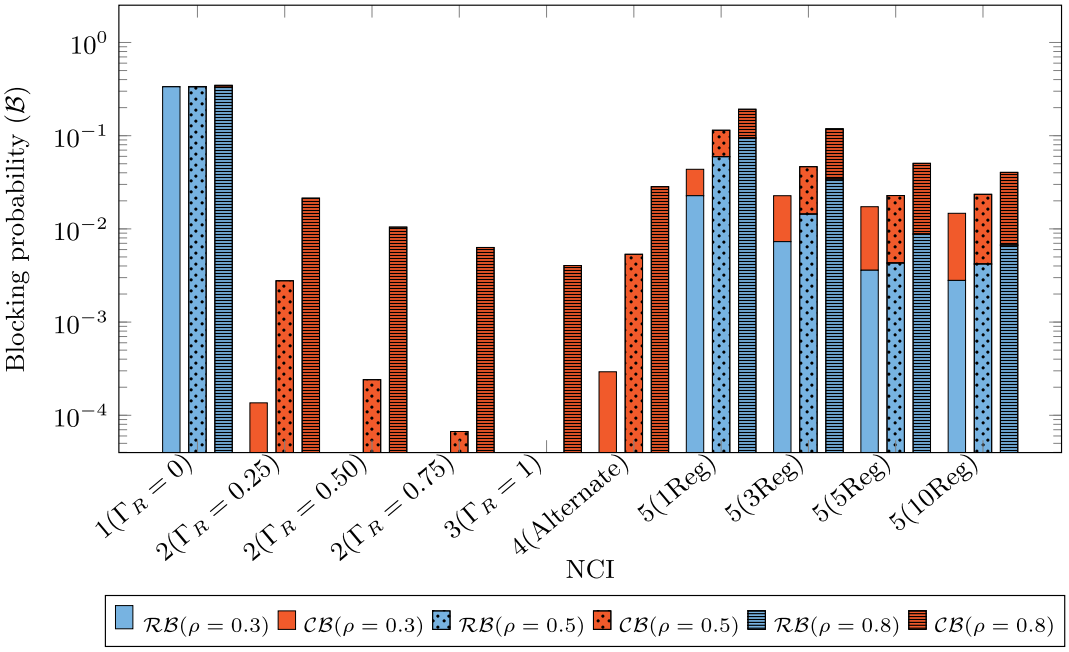

FIGURE 6. Sources of blocking -reach blocking ($\mathcal{RB}$) and capacity blocking ($\mathcal{CB}$)- for every network configuration.

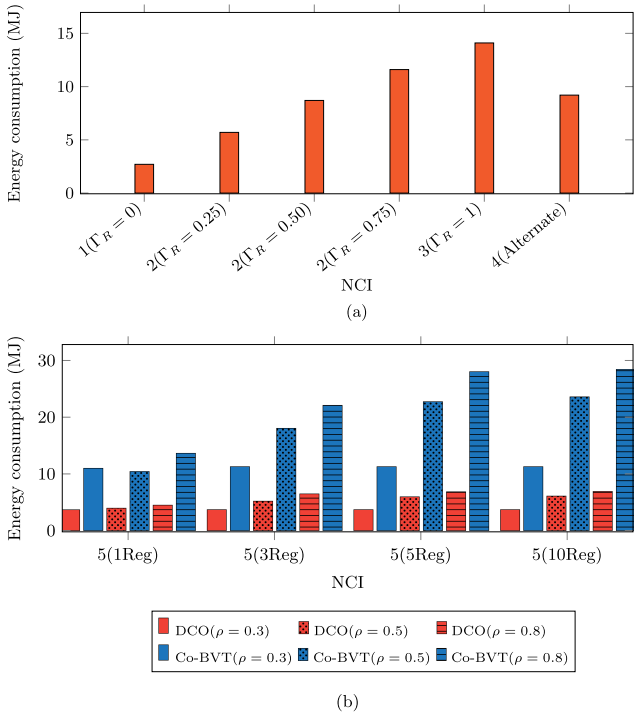

FIGURE 7. Network energy consumption considering T = 1000 s.

Among the transparent network configurations (NCI 1-4), NCI 1 presents the lowest SE, equal to 2.65 b/s/Hz. Compared to NCI 1, SE has increased in NCI 2, 3, and 4 thanks to Raman amplification. The higher the value of the factor Γ_R, the higher the observed SE (with NCI 4 achieving a spectral efficiency similar to NCI 2 with $\Gamma_R = 0.25$). As shown in Fig. 8 **(b)**, this behavior occurs because the use of a higher Raman gain ratio allows for more efficient modulation formats, as PM-16-QAM and PM-64-QAM, to be used. For example, for NCI 1, only 8% of connections were established using PM-16-QAM, and the remaining 92% of them were established using PM-QPSK. Instead, in the case of NCI 3 ($\Gamma_R = 1$) 51%, 45% and 4% of the connections used PM-QPSK, PM-16-QAM and PM-64-QAM, respectively. These percentages explain the observed increase in the spectral efficiency of the network in NCI 3 compared to the NCI 1 shown in Fig. 8 **(a)**.

Notice that the maximum achievable SE is 3.2 b/s/Hz, which is lower than the SE achieved using QSPK over two polarizations. This value can be explained considering the requested bit rates used in the simulations, the available modulation formats, and the constraints of EONs that an established connection uses a minimum of 1 FSU. The simulated bit rate requests were 10, 40, 100, 400 and 1000 Gb/s. In particular, bit rates of 10, 40 Gb/s require less than a single FSU of optical bandwidth using the modulation formats under consideration, which reduces the overall SE as no other connections are established using the same FSU. Remark that, due to the uniform traffic distribution assumed in this work, 10 and 40 Gb/s represent 40% of the simulated connection requests.

For the translucent configuration (NCI 5), only a slight improvement compared to NCI 1 is observed. In this case, a SE of 2.675 b/s/Hz was obtained, 0.025 b/s/Hz higher than NCI 1. That is, the use of regenerators to increase the reach of a connection does not lead to a more significant usage of more efficient modulation formats, as shown in Fig. 8 **(b)**,

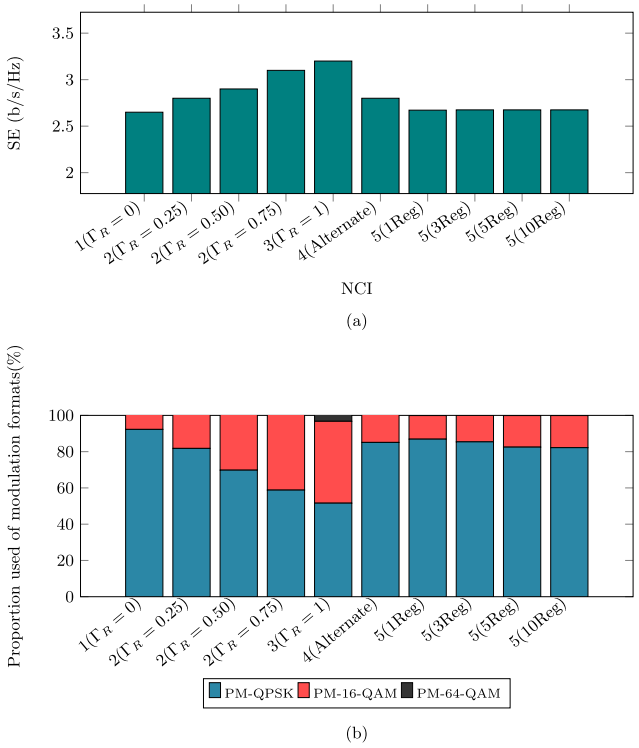

FIGURE 8. Spectral efficiency of the network for every NCI for a traffic load of 0.3.

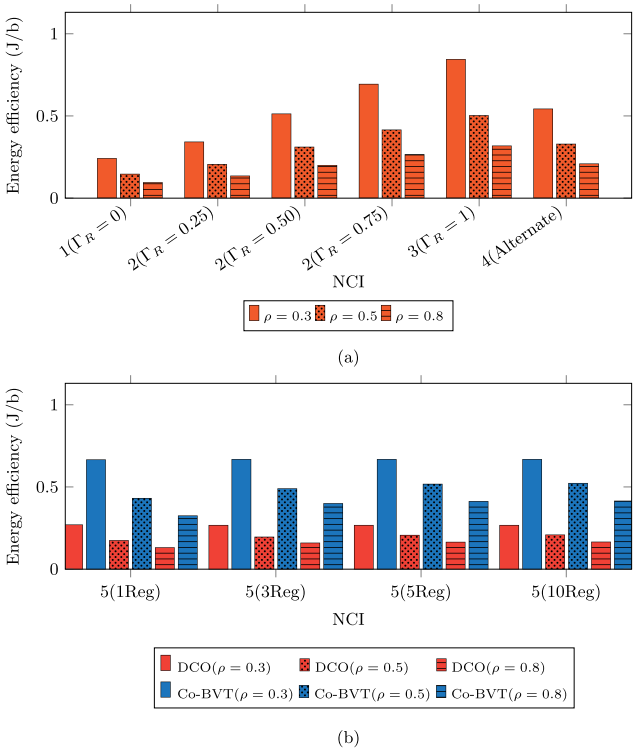

FIGURE 9. Energy efficiency of the network for every NCI.

where a maximum of 17% of PM-16-QAM connections is observed for NCI 5. This behavior is explained considering the limited number of regenerators per node, which translates into a maximum number of regenerated connections that can be established simultaneously. Thus, only a fraction of established connections could use modulation formats more efficiently than NCI 1. In particular, approximately 30 % of the established connections use regenerators, and only 30% of those connections can improve their SE using PM-16-QAM due to the reach limitations of the studied formats. The network SE obtained for traffic loads of 0.5 and 0.8 was similar to that shown in Fig. 8 **(a)** for a traffic load of 0.3. In particular, the same trend was observed when changing the NCI.

The energy efficiency of every network configuration is shown in Fig. 9 considering traffic loads of 0.3, 0.5, and 0.8. Fig. 9 **(a)** presents the energy efficiency for NCI 1-4, and Fig. 9 **(b)** for NCI 5. Similar to Fig.7 **(a)**, for NCI 1-4 a higher energy per bit is required as the Γ_R increases from 0 to 1 for all traffic loads. For every NCI, as the traffic load increases, the required energy per bit is reduced due to the greater throughput in the network. As the required energy for the transparent scenarios (NCI 1-4) is constant, the energy efficiency varies only according to the number of established connections.

Unlike amplifiers, regenerators only consume energy when they are operative. As seen in Fig. 7 **(b)**, both the traffic load and the number of available regenerators increase the overall energy consumption, and the number of established connections will determine the energy efficiency. For a traffic load of 0.3, we observe a constant energy per bit of 0.267 and 0.666 J/b for the DCO and Co-BVT, respectively. As the traffic load increments, the required energy per bit is reduced as a greater throughput is established in the network.

Noticeably, NCI 1 presents the best energy efficiency for all traffic loads. However, it offers the highest blocking probability. The use of regenerators (NCI 5) will strongly depend on the deployed technology, with the DCO transceiver offering a consumed energy per bit similar to NCI 1 (0.27 J/b). The Co-BVT presents a consumed energy per bit comparable to NCI 2 with $\Gamma_R = 0.5$, and the latter offers considerably lower blocking probabilities.

D. FINAL CONSIDERATION

The network configuration, in terms of the amplification and regeneration scheme selected, impacts the service performance parameters directly in the service level agreement for optical networks (O-SLA) [48] subscribed between a service provider and a subscriber, in particular the throughput. Since the network operator aims to reduce energy consumption while meeting the specified values of the O-SLA, the best amplification and regeneration scheme will be determined by the quality of service required by connections. For example, in a network serving high-throughput connections, NCI 3 would be the best choice. However, this is also the configuration with the highest energy consumption. Instead,

connections with meager throughput requirements could be served with the lowest energy consumption NCI 1.

V. CONCLUSION

We have studied the impact of the physical layer implementation on the blocking probability and energy consumption of dynamic EONs, using two network topologies and considering transparent and translucent network configurations. The transparent configurations were all-EDFA, hybrid Raman-EDFA, all-DFRA, and alternating EDFA and DFRA spans, termed NCI 1-4. The translucent configuration, termed NCI 5, used all-EDFA amplification and a limited number of 3R regenerators in each node.

For NSFNet and UKNet topologies, the blocking probability of NCI 1 was the highest of the studied configurations, followed by NCI 5 and 4. NCI 2 and 3 offered the lowest blocking probability, which decreased as the Raman gain ratio (Γ_R) was increased. For NSFNet, the limited reach dominated the blocking in NCI 1 and 5 (reach blocking) of the available modulations formats, while for NCI 2, 3, and 4, the blocking was driven by lack of capacity (capacity blocking). On the other hand, for UKNet the blocking in all NCI is associated with capacity blocking; due to shorter routes there is no reach blocking, and more complex modulation formats are used. In general, as the blocking probability was reduced, all studied NCI improved their spectral efficiency using more complex modulation formats. For the two topologies, NCI 1 was shown to be the most efficient configuration in terms of energy consumption, while the total consumed energy increased linearly with the Γ_R for NCI 2 and 3. The energy consumption of NCI 4 was shown to be similar to NCI 2 with $\Gamma_R = 0.75$. The use of 3R regenerators in NCI 5 represented an increase in energy consumption relative to NCI 1. In the case of the UKNet, this behavior is observed for moderate to high traffic loads. For low traffic loads, 3R regenerators are not used at all. Furthermore, the technology used in the regenerators has a meaningful impact on the total consumed energy and the energy efficiency of the network. Finally, we identify NCI 2 with $\Gamma_R = 0.25$ as a promising alternative to reduce the blocking probability significantly in wide-area EONs, such as NSFNet, without a prohibitive increase in energy consumption, with a factor of 2.1, and energy efficiency, with a factor of 1.4, compared to NCI 1, as long as the O-SLA requirements are met. Notice that this recommendation is not based on financial considerations. We remark that the financial benefit-cost should inform the final decision made by a network operator of any alternative: an alternative will be feasible only if the financial benefit of decreasing the blocking ratio (due to increased revenue) compensates for the increased cost related to energy consumption.

The above-discussed results have been obtained under simplified models that impose some limitations on the work. Regarding the limitations of the physical layer model, Raman and hybrid amplifiers assume ideal depolarized pump sources and lossless coupling components, which might result in a lower equivalent noise figure than practical components. All network configurations (NCI 1-5) assume that the ASE noise is an Additive White Gaussian Noise process and do not consider wavelength-dependent noise and gain, which might lead to a different reach for every multiplexed channel. Other assumptions described in the manuscript include ideal network components and ideal compensation of linear impairments using digital signal processing. Despite all the mentioned limitations, a 2 dB margin for the amplifier gain in each network configuration was included to reduce the impact of the limitations mentioned herein.

In future work, we will extend our analysis to multiband and multicore transmission systems, two promising alternatives to enlarge the capacity of optical networks. In such systems, new physical impairments need to be considered (stimulated Raman scattering in multiband systems and inter-core cross-talk in multicore fibers) that might affect the network performance. We will also focus on including the regenerator/HFA placement problem in the study.

REFERENCES

[1] O. Gerstel, M. Jinno, A. Lord, and S. J. B. Yoo, "Elastic optical networking: A new dawn for the optical layer?" *IEEE Commun. Mag.*, vol. 50, no. 2, pp. 12–20, Feb. 2012.

[2] H. Waldman, "The impending optical network capacity crunch," in *Proc. Int. Opt. Photon. Conf. (SBFoton IOPC)*, Oct. 2018, pp. 1–3.

[3] *Spectral Grids for WDM Applications: DWDM Frequency Grid*, document ITU-T G.694.1, Telecommunication Standardization Sector of ITU, Ginebra, Switzerland, 2012.

[4] B. Chatterjee and E. Oki, *Elastic Optical Networks: Fundamentals, Design, Control, and Management*. Boca Raton, FL, USA: CRC Press, 2020.

[5] A. Fontinele, I. Santos, J. N. Neto, D. R. Campelo, and A. Soares, "An efficient IA-RMLSA algorithm for transparent elastic optical networks," *Comput. Netw.*, vol. 118, pp. 1–14, May 2017.

[6] F. S. Abkenar and A. G. Rahbar, "Study and analysis of routing and spectrum allocation (RSA) and routing, modulation and spectrum allocation (RMSA) algorithms in elastic optical networks (EONs)," *Opt. Switching Netw.*, vol. 23, pp. 5–39, Jan. 2017.

[7] V. A. C. Vale and R. C. Almeida, "Power, routing, modulation level and spectrum assignment in all-optical and elastic networks," *Opt. Switching Netw.*, vol. 32, pp. 14–24, Apr. 2019.

[8] S. Araujo, A. Soares, A. Fontinele, D. R. Campelo, J. V. dos Reis, and E. Barbosa, "Circuit reallocation strategy aware of the physical layer effects for elastic optical networks," in *Proc. IEEE Symp. Comput. Commun. (ISCC)*, Jun. 2018, pp. 970–975.

[9] F. I. Calderón, A. Lozada, D. Bórquez-Paredes, R. Olivares, E. J. Davalos, G. Saavedra, N. Jara, and A. Leiva, "BER-adaptive RMLSA algorithm for wide-area flexible optical networks," *IEEE Access*, vol. 8, pp. 128018–128031, 2020.

[10] B. C. Chatterjee, N. Sarma, and E. Oki, "Routing and spectrum allocation in elastic optical networks: A tutorial," *IEEE Commun. Surveys Tuts.*, vol. 17, no. 3, pp. 1776–1800, Aug. 2015.

[11] B. C. Chatterjee, S. Ba, and E. Oki, "Fragmentation problems and management approaches in elastic optical networks: A survey," *IEEE Commun. Surveys Tuts.*, vol. 20, no. 1, pp. 183–210, 1st Quart., 2018.

[12] L. R. Costa, I. B. Brasileiro, and A. C. Drummond, "Low margin QoT-aware RMLSA with circuit invigoration in elastic optical networks," in *Proc. IEEE Global Commun. Conf. (GLOBECOM)*, Dec. 2020, pp. 1–6.

[13] X. Luo, Y. Zhao, X. Chen, L. Wang, M. Zhang, J. Zhang, Y. Ji, H. Wang, and T. Wang, "Manycast routing, modulation level and spectrum assignment over elastic optical networks," *Opt. Fiber Technol.*, vol. 36, pp. 317–326, Jul. 2017.

[14] B. Li and Y.-C. Kim, "Efficient routing and spectrum allocation considering QoT in elastic optical networks," in *Proc. 38th Int. Conf. Telecommun. Signal Process. (TSP)*, Jul. 2015, pp. 109–112.

[15] T. Hashimoto, K.-I. Baba, and S. Simojo, "A study on routing, modulation level, and spectrum allocation algorithms for elastic optical path networks," in *Proc. IEEE 3rd Int. Conf. Photon.*, Oct. 2012, pp. 395–399.
[16] M. Klinkowski, K. Walkowiak, and M. Jaworski, "Off-line algorithms for routing, modulation level, and spectrum assignment in elastic optical networks," in *Proc. 13th Int. Conf. Transparent Opt. Netw.*, Jun. 2011, pp. 1–6.
[17] W. S. Pelouch, "Raman amplification: An enabling technology for long-haul coherent transmission systems," *J. Lightw. Technol.*, vol. 34, no. 1, pp. 6–19, Jan. 1, 2016.
[18] A. Fallahpour, H. Beyranvand, S. A. Nezamalhosseini, and J. A. Salehi, "Energy efficient routing and spectrum assignment with regenerator placement in elastic optical networks," *J. Lightw. Technol.*, vol. 32, no. 10, pp. 2019–2027, May 2014.
[19] J. Pedro and N. Costa, "Optimized hybrid Raman/EDFA amplifier placement for DWDM mesh networks," *J. Lightw. Technol.*, vol. 36, no. 9, pp. 1552–1561, May 1, 2018.
[20] A. Ferrari, M. Cantono, A. Ahmad, and V. Curri, "Physical layer strategies to save lightpath regenerators," *IEEE/OSA J. Opt. Commun. Netw.*, vol. 10, no. 9, pp. 703–711, Sep. 2018.
[21] M. Aibin and K. Walkowiak, "Adaptive modulation and regenerator-aware dynamic routing algorithm in elastic optical networks," in *Proc. IEEE Int. Conf. Commun. (ICC)*, Jun. 2015, pp. 5138–5143.
[22] M. Cantono, A. Ferrari, U. Waheed, A. Ahmad, S. M. H. Zaidi, A. Bianco, and V. Curri, "Networking benefit of hybrid fiber amplification for light-path regenerators saving," in *Proc. Opt. Fiber Commun. Conf.*, 2017, Paper W4F.7.
[23] E. F. da Silva, R. C. Almeida, H. A. Pereira, and D. A. R. Chaves, "Assessment of novel regenerator assignment strategies in dynamic translucent elastic optical networks," *Photonic Netw. Commun.*, vol. 39, no. 1, pp. 54–69, Feb. 2020.
[24] A. Ahmad, A. Bianco, H. Chouman, G. Marchetto, S. Tahir, and V. Curri, "Impact of fiber type and Raman pumping in NyWDM flexible-grid elastic optical networks," in *Proc. 18th Int. Conf. Transparent Opt. Netw. (ICTON)*, Jul. 2016, pp. 1–4.
[25] A. Ahmad, A. Bianco, V. Curri, G. Marchetto, and S. Tahir, "Raman pumping as an energy efficient solution for NyWDM flexible-grid elastic optical networks," *Int. J. Electr. Comput. Eng.*, vol. 7, no. 5, p. 2627, Oct. 2017.
[26] H.-C. Le, N. T. Dang, and N. Duc Nguyen, "Impact of optical regeneration on dynamic elastic optical networks," in *Proc. Int. Conf. Adv. Technol. Commun. (ATC)*, Oct. 2017, pp. 11–15.
[27] D. Borquez-Paredes, F. Calderon, N. Jara, A. Leiva, A. Lozada, R. Olivares, and G. Saavedra, "3R regeneration in elastic optical networks and its impact on the network quality of service," in *Proc. 22nd Int. Conf. Transparent Opt. Netw. (ICTON)*, Jul. 2020, pp. 1–4.
[28] G. P. Agrawal, "Optical communication: Its history and recent progress," in *Optics in Our Time*. Cham, Switzerland: Springer, 2016, pp. 177–199.
[29] D. Semrau, G. Saavedra, D. Lavery, R. I. Killey, and P. Bayvel, "A closed-form expression to evaluate nonlinear interference in Raman-amplified links," *J. Lightw. Technol.*, vol. 35, no. 19, pp. 4316–4328, Oct. 1, 2017.
[30] P. Poggiolini, G. Bosco, A. Carena, V. Curri, Y. Jiang, and F. Forghieri, "The GN-model of fiber non-linear propagation and its applications," *J. Lightw. Technol.*, vol. 32, no. 4, pp. 694–721, Feb. 15, 2014.
[31] V. Curri, A. Carena, P. Poggiolini, G. Bosco, and F. Forghieri, "Extension and validation of the GN model for non-linear interference to uncompensated links using Raman amplification," *Opt. Exp.*, vol. 21, no. 3, pp. 3308–3317, 2013.
[32] A. Mitra, D. Ives, A. Lord, P. Wright, and S. Kar, "Non-linear impairment modeling for flexgrid network and its application in offline network equipment upgrade strategy," in *Proc. Int. Conf. Opt. Netw. Design Modeling (ONDM)*, May 2015, pp. 57–62.
[33] D. Ives, P. Bayvel, and S. Savory, "Adapting transmitter power and modulation format to improve optical network performance utilizing the Gaussian noise model of nonlinear impairments," *J. Lightw. Technol.*, vol. 32, no. 21, pp. 3485–3494, Nov. 1, 2014.
[34] L. M. Zhang and F. R. Kschischang, "Staircase codes with 6% to 33% overhead," *J. Lightw. Technol.*, vol. 32, no. 10, pp. 1999–2002, May 15, 2014.
[35] L. Lundberg, P. A. Andrekson, and M. Karlsson, "Power consumption analysis of hybrid EDFA/Raman amplifiers in long-haul transmission systems," *J. Lightw. Technol.*, vol. 35, no. 11, pp. 2132–2142, Jun. 1, 2017.
[36] J. López, Y. Ye, V. López, F. Jiménez, R. Duque, and P. M. Krummrich, "On the energy efficiency of survivable optical transport networks with flexible-grid," in *Proc. Eur. Conf. Exhib. Opt. Commun.*, 2012, p. P5-05.
[37] J. Zhang, Y. Zhao, X. Yu, J. Zhang, M. Song, Y. Ji, and B. Mukherjee, "Energy-efficient traffic grooming in sliceable-transponder-equipped IP-over-elastic optical networks [Invited]," *J. Opt. Commun. Netw.*, vol. 7, no. 1, pp. A142–A152, 2015.
[38] G. A. Beletsioti, G. I. Papadimitriou, P. Nicopolitidis, E. Varvarigos, and S. Mavridopoulos, "A learning-automata-based congestion-aware scheme for energy-efficient elastic optical networks," *IEEE Access*, vol. 8, pp. 101978–101992, 2020.
[39] J. Halder, T. Acharya, M. Chatterjee, and U. Bhattacharya, "E-S-RSM-RSA: A novel energy and spectrum efficient regenerator aware multipath based survivable RSA in offline EON," *IEEE Trans. Green Commun. Netw.*, vol. 5, no. 3, pp. 1451–1466, Sep. 2021.
[40] J. M. H. Elmirghani, T. Klein, K. Hinton, T. E. H. El-Gorashi, A. Q. Lawey, and X. Dong, "GreenTouch GreenMeter core network power consumption models and results," in *Proc. IEEE Online Conf. Green Commun. (OnlineGreenComm)*, Nov. 2014, pp. 1–8.
[41] H. Zhang, B. Zhu, S. Park, C. Doerr, M. Aydinlik, J. Geyer, T. Pfau, G. Pendock, R. Aroca, F. Liu, and C. Rasmussen, "Real-time transmission of 16 Tb/s over 1020 km using 200 Gb/s CFP2-DCO," *Opt. Exp.*, vol. 26, no. 6, p. 6943, 2018.
[42] J. Geyer, C. Rasmussen, B. Shah, T. Nielsen, and M. Givehchi, "Power efficient coherent transceivers," in *Proc. 42nd Eur. Conf. Opt. Commun. (ECOC)*, 2016, pp. 1–3.
[43] P. J. Winzer, "High-spectral-efficiency optical modulation formats," *J. Lightw. Technol.*, vol. 30, no. 24, pp. 3824–3835, Dec. 15, 2012.
[44] R. S. Tucker, R. Parthiban, J. Baliga, K. Hinton, R. W. A. Ayre, and W. V. Sorin, "Evolution of WDM optical IP networks: A cost and energy perspective," *J. Lightw. Technol.*, vol. 27, no. 3, pp. 243–252, Feb. 1, 2009.
[45] R. S. Tucker, "Green optical communications—Part I: Energy limitations in transport," *IEEE J. Sel. Topics Quantum Electron.*, vol. 17, no. 2, pp. 245–260, Mar. 2011.
[46] D. Eppstein, "Finding the K shortest paths," *SIAM J. Comput.*, vol. 28, no. 2, pp. 652–673, 1999.
[47] Ì. Brasileiro, J. Valdemir, and A. Soares, "Regenerator assignment with circuit invigorating," *Opt. Switching Netw.*, vol. 34, pp. 58–66, Nov. 2019.
[48] W. Fawaz, B. Daheb, O. Audouin, M. Du-Pond, and G. Pujolle, "Service level agreement and provisioning in optical networks," *IEEE Commun. Mag.*, vol. 42, no. 1, pp. 36–43, Jan. 2004.

ASTRID LOZADA received the M.Sc. degree in electronic engineering from Universidad Técnica Federico Santa María (UTFSM), Chile, in 2020, where she is currently pursuing the Ph.D. degree in electronic engineering. Her research interests include fiber optic communication systems and nonlinear fiber effects.

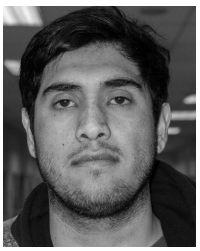

FELIPE CALDERÓN received the B.Sc. degree in electronic engineering from the Pontificia Universidad Católica de Valparaíso (PUCV), Chile, in 2020, where he is currently pursuing the M.Sc. degree in electrical engineering. His current interests include optical networking and machine learning.

JOSÉ NÚÑEZ KASANEVA received the B.Sc. degree in electrical engineering from the Universidad de Concepción (UDEC), Chile, in 2021, where he is currently pursuing the M.Sc. degree in electrical engineering. His current interests include elastic optical networks, optical network survivability, machine learning, and optimization.

DANILO BÓRQUEZ-PAREDES received the B.Eng. degree in telematics engineering from Universidad Técnica Federico Santa María (UTFSM), Valparaiso, Chile, in 2012, and the Ph.D. degree from Universidad Adolfo Ibañez, in September 2018. He also received the professional title in telematics engineering from UTFSM. He is currently a full-time Professor with the Faculty of Engineering and Sciences, Universidad Adolfo Ibañez. His research interests include the dynamic allocation of resources in flexible optical networks, network virtualization, graph theory, and optimization.

RICARDO OLIVARES received the B.Sc. degree in electronic engineering from Universidad Técnica Federico Santa María (UTFSM), Chile, in 1983, and the M.Sc. and D.Sc. degrees in electrical engineering from the Pontificia Universidade Católica do Rio de Janeiro, Brazil, in 1994 and 2001, respectively. He has been with the Department of Electronic Engineering, UTFSM, since 1986, where he is currently an Assistant Professor. His current interests include RF measurements, fiber optic communication systems, fiber optical sensors, and nonlinear fiber optics.

ALEJANDRA BEGHELLI received the B.Eng. degree in electronic engineering and the M.Sc. degree from Universidad Técnica Federico Santa María, Chile, in 1996 and 2001, respectively, and the Ph.D. degree from University College London (UCL), London, U.K. in 2006. She is currently a Lecturer with the Department of Electronic and Electrical Engineering, UCL. Her current research interests include dynamic resource allocation in optical networks, with an emphasis on the application of artificial intelligence techniques.

NICOLÁS JARA (Member, IEEE) received the B.Sc. and M.Sc. degrees in telematics engineering from Universidad Técnica Federico Santa María (UTFSM), Chile, in 2010, and the Ph.D. degree from the Université de Rennes I, France, in 2017, and UTFSM, in 2018. He is currently an Assistant Professor with the Department of Electronics, UTFSM. His current research interests include optical networks design, networks performability, and simulation techniques.

ARIEL LEIVA (Member, IEEE) received the B.Sc. degree in electronic engineering and the M.Sc. degree in electrical engineering from the Pontificia Universidad Católica de Valparaíso (PUCV), Chile, in 2003 and 2007, respectively, and the Ph.D. degree from Universidad Técnica Federico Santa María, Valparaiso, Chile, in 2013. He is currently a Lecturer with PUCV. His current interests include fiber optic communication systems and optical networking.

GABRIEL SAAVEDRA (Member, IEEE) received the B.Eng. degree in telecommunication engineering and the M.Sc. degree from the Universidad de Concepción, Chile, in 2013 and 2014, respectively, and the Ph.D. degree from University College London (UCL), London, U.K., in 2019. He is currently an Associate Professor with the Universidad de Concepción. His research interests include nonlinear fiber effects, nonlinear compensation methods, and digital signal processing for optical communications.